Reconstruction of the sum-rule-constrained classical binary-collision model for inner-shell ionizations

C. M. Kwei and Y. F. Chen
Department of Electronics Engineering, National Chiao Tung University, Hsinchu, Taiwan

C. J. Tung
Institute of Nuclear Science, National Tsing Hua University, Hsinchu, Taiwan

(Received 4 September 1991)

Tung has constructed a sum-rule-constrained classical binary-collision model for the estimation of generalized oscillator strengths (GOS's) of the 1*s* and 2*s* subshells of atoms. He applied three sum rules to determine the momentum-dependent parameters introduced in the GOS function based on the classical binary-collision model. Several deficiencies have then been found regarding these sum rules that adopted the less accurate hydrogenic model and included the unwanted contribution from discrete excitations. In the present work, we have reconstructed this model by employing improved sum rules obtained from Hartree-Fock-Slater matrix element calculations. The refined model has been successfully applied to estimate ionization generalized oscillator strengths of atomic *K* and *L* shells.

PACS number(s): 32.70.Cs, 34.50.Fa

I. INTRODUCTION

Studies on the dynamic response of an atom in its inelastic interactions with a charged particle stem from the increasing need for reliable cross sections in such applications as electron microscopy, radiology, nuclear physics, solid-state physics, radiation physics, etc. [1,2]. The generalized oscillator strength (GOS) introduced by Bethe [3] characterizes this response in terms of the momentum- and energy-dependent response function. Although the GOS may be contributed to by excitations and ionizations, it is the latter contribution that is most important in determining inelastic cross sections.

Much effort has been made in the past to work out simple yet reliable methods for the estimation of ionization GOS's. The classical binary-collision (CBC) model [4–6] and the local plasma approximation [7–9] (LPA) are the frequently quoted methods. Unfortunately, they are useful only for the limited range of energy and momentum transfers. Tung [10] has previously constructed a sum-rule-constrained CBC model that increased the accuracy of ionization GOS's of the CBC model. He applied three sum rules to determine the momentum-dependent parameters introduced in the GOS function based on the CBC model. Several deficiencies have then been found regarding these sum rules that adopted the less accurate hydrogenic model and included the unwanted contribution from discrete excitations. Because of these deficiencies, the sum-rule-constrained model works only fairly for the 1*s* and 2*s* subshells but poorly for the 2*p* subshell. In the present work, we have reconstructed this model by employing improved sum rules obtained from Hartree-Fock-Slater (HFS) matrix element calculations [11–13]. The reconstructed model has been successfully applied to ionization GOS's of the *K* and *L* shells. It was found that the agreement on ionization GOS's between the present work and the HFS matrix element data was excellent for all momentum and energy transfers.

II. THEORY

A. Classical binary-collision model

The ionization GOS's per atom of the CBC model using a hydrogenic speed distribution for atomic electrons in the *i*th subshell is given by [10]

$$\left[\frac{df}{d\epsilon}\right]_{\rm CBC}=\frac{Z_i 2^8\epsilon\eta^3\theta(\epsilon-\epsilon_i)}{3\pi[(\epsilon-\eta^2)^2+4\eta^2]^3}\ , \tag{1}$$

where $\eta=\hbar k/(2mE_{0i})^{1/2}$, $\epsilon=\hbar\omega/E_{0i}$, and $\epsilon_i=\hbar\omega_i/E_{0i}$ are dimensionless variables related to, respectively, the momentum transfer $\hbar k$, the energy transfer $\hbar\omega$, and the binding energy $\hbar\omega_i$ for the *i*th subshell; E_{0i} is the mean kinetic energy of electrons in the *i*th subshell; Z_i is the number of electrons per atom in the *i*th subshell; and θ is the step function. For a given (n,l) subshell, the mean kinetic energy may be estimated by the Slater rule [14] as

$$E_0(n,l)=(Z_{\rm eff}/n^*)^2\mathcal{R}\ , \tag{2}$$

where $\mathcal{R}\approx 13.6$ eV is the Rydberg energy constant and $n^*=1$, 2, 3, 3.7, 4, and 4.2 corresponding to $n=1$, 2, 3, 4, 5, and 6, respectively. The effective nuclear charge acted upon electrons in the (n,l) subshell is given by

$$Z_{\rm eff}=Z-0.35(Z_{n,l}-1)-\sum_{i=1}^{n-1}\sum_{j=0}^{i-l}Z_{i,j}+\delta_{l,0}\left[0.15\sum_{j=0}^{n-2}Z_{n-1,j}-0.35Z_{n,1}\right]$$
$$+0.05\delta_{n,1}\delta_{l,0}(Z_{1,0}-1)+\delta_{l,1}\left[0.15\sum_{j=0}^{n-2}Z_{n-1,j}-0.35Z_{n,0}\right]\ , \tag{3}$$

where Z is the atomic number, $Z_{i,j}$ is the number of electrons in the (i,j) state, and $\delta_{i,j}$ is the Kronecker δ function.

It is seen that the GOS in Eq. (1) approaches zero at the optical end, i.e., $\eta \rightarrow 0$. This is a critical deficiency compared to the finite optical GOS data measured experimentally. To remedy this deficiency, we have retained the basic form of Eq. (1) but added to it several terms according to [10]

$$\frac{df}{d\epsilon} = \left[\frac{df}{d\epsilon}\right]_{\text{CBC}} [A(\eta)+\epsilon B(\eta)+\epsilon^2 C(\eta)] , \tag{4}$$

where A, B, and C are the momentum-dependent parameters to be determined using the various sum rules of the ionization GOS moments defined by

$$S_\eta^I(\mu) = \int \epsilon^\mu \frac{df}{d\epsilon} d\epsilon . \tag{5}$$

Note that we have included in Eq. (4) terms up to ϵ^2. Any higher-order terms would result in an unsatisfactorily asymptotic behavior of the GOS at very large ϵ [15].

B. Sum rules

The three sum rules applied by Tung were [16]

$$S_\eta^I(-1) = Z_i[1-(1+\eta^2/4)^{-4}]/\eta^2 , \tag{6}$$

$$S_\eta^I(0) = Z_i , \tag{7}$$

and

$$S_\eta^I(1) = Z_i[\eta^2+\tfrac{4}{3}] . \tag{8}$$

These sum rules were established under the assumptions of (a) adopting the less accurate hydrogenic model and (b) including the contribution from discrete excitations.

To test the validity of the above assumptions and the accuracy of Eq. (1), we compare in Fig. 1 results of $S_\eta^I(0)$ calculated using Eq. (7), Eq. (1), and the HFS matrix element method [11] for $1s$, $2s$, and $2p$ subshells of the oxygen atom. It is shown that all results approach the electron occupation number Z_i at large momentum transfers. The CBC model of Eq. (1) leads to dashed curves which underestimate $S_\eta^I(0)$ at very small momentum transfers but overestimate it at moderate momentum transfers as compared to the HFS data (solid curves). It will be discussed later that assumptions behind Eq. (7) lead to a constant oscillator strength at any momentum transfers (dot-dash curves). By comparing results of solid and dot-dash curves, exchange of the oscillator strength predicted by Eq. (7) from one subshell to another is shown. Such an exchange, enhanced at small momentum transfers, tends to remove oscillator strength from the tightly bound $2s$ subshell to the loosely bound $2p$ subshell.

Theoretically, the zero-order sum rule for the ith subshell of an atom is given by the independent-electron model as [17,18]

$$S(0) = S_\eta^I(0)+S_\eta^U(0)+S_\eta^0(0) = Z_i , \tag{9}$$

where $S(0)$, $S_\eta^I(0)$, $S_\eta^U(0)$, and $S_\eta^0(0)$ are, respectively, the oscillator strength associated with the total (ionizations and excitations), ionizations, excitations to unoccupied levels, and excitations to occupied levels. Comparing Eq. (9) with Eq. (7), one sees that the ionization sum rule of Eq. (7) contains the unwanted contribution from excitations. Such a contribution becomes negligibly small at large momentum transfers, so that Eq. (7) holds. Note that excitations to occupied states are not excluded in the independent-electron model. Those excitations to the lower and upper occupied states, corresponding to radiation emissions and absorptions, respectively, contribute to $S_\eta^0(0)$ negative and positive oscillator strengths [19]. The total contribution by excitations to occupied levels can be negative for an outer subshell where excitations to lower occupied states dominate. Although, in reality, excitations to occupied states do not exist due to the exclusion principle, such an exclusion has no net effect on the total oscillator strength of an atom due to the cancellation of $S_\eta^0(0)$ after summing over all subshells. The exchange of ionization oscillator strength predicted by Eq. (7) from one subshell to another follows Eq. (9).

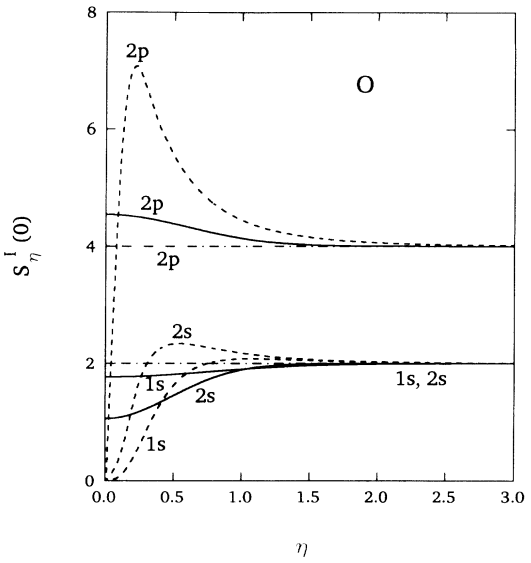

FIG. 1. A plot of the $\mu=0$ moment of the ionization GOS's, defined in Eq. (5), for oxygen $1s$, $2s$, and $2p$ subshells as a function of momentum transfer. The solid, dot-dash, and dashed curves represent, respectively, results of the HFS matrix element method, Eq. (7), and Eq. (1).

Similarly, we compare in Fig. 2 results of $S_\eta^I(-1)$ using the various methods for the $2s$ subshell of a nitrogen atom. Again, the CBC model of Eq. (1) yields values (dashed curves) underestimating, overestimating, and approaching the HFS data (solid curves) at small, moderate, and large momentum transfers. The application of Eq. (6), corresponding to the hydrogenic model, leads to results (dot-dash curves) somewhat larger than the HFS data at small momentum transfers. Finally, we compare in Fig. 3 results of $S_\eta^I(1)$ using the various methods for the $2p$ subshell of a carbon atom. In this case, the CBC model of Eq. (1) (dashed curves) still fails to predict the correct sum rule at small momentum transfers. The slight difference between the results of Eq. (8) (dot-dash

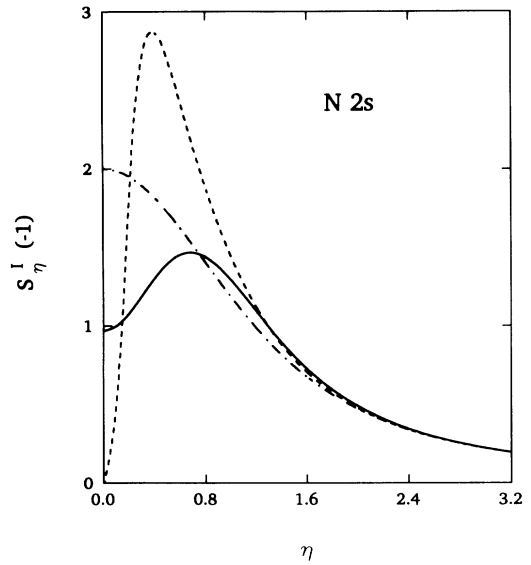

FIG. 2. A plot of the $\mu=-1$ moment of the ionization GOS, defined in Eq. (5), for the nitrogen $2s$ subshell as a function of momentum transfer. The solid, dot-dash, and dashed curves represent, respectively, results of the HFS matrix element method, Eq. (6), and Eq. (1).

curves) and the HFS data (solid curves) indicates that those assumptions listed under Eq. (8) are better applicable to ionization GOS's at large energy transfers. Based on these comparisons, we conclude that the CBC model of Eq. (1) fails to predict the ionization GOS at small momentum transfers. In addition, Eqs. (6)–(8) are ineffective in determining the parameters involved in Eq. (4).

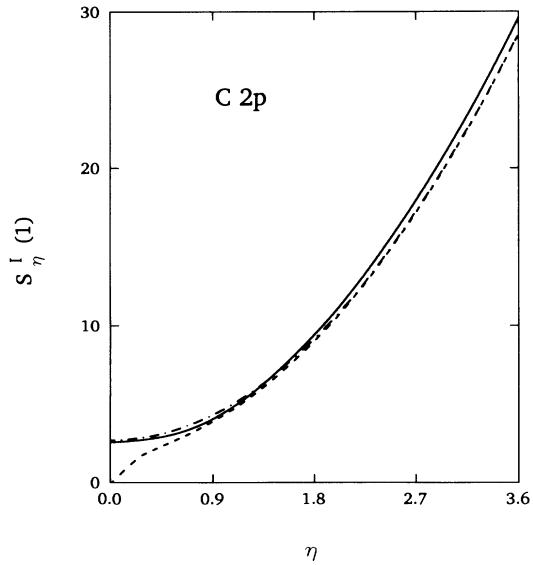

FIG. 3. A plot of the $\mu=1$ moment of the ionization GOS, defined in Eq. (5), for the carbon $2p$ subshell as a function of momentum transfer. The solid, dot-dash, and dashed curves represent, respectively, results of the HFS matrix element method, Eq. (8), and Eq. (1).

C. Sum-rule-constrained ionization (GOS)

In this work, we apply Eq. (4) by employing three sum rules, i.e., $S_\eta^I(-1)$, $S_\eta^I(0)$, and $S_\eta^I(1)$, evaluated by the HFS matrix element method [11]. For analytical manipulations, we fit these sum rules to expressions constructed with the guidance of Eqs. (6)–(8). Constants introduced to these expressions are dependent on the subshell and the atom of interest. It is found that $S_\eta^I(0)$ is satisfactorily fitted to the expression

$$S_\eta^I(0)=Z_i[1-A_i\exp(-B_i\eta^2)]\ , \tag{10}$$

with $A_i=0.06+0.007Z$, $0.653-0.023Z$, $-0.046-0.011Z$ and $B_i=0.562+0.04Z$, $0.855+0.165Z$, $-1.01+0.301Z$ for the $i=1s$, $2s$, and $2p$ subshell, respectively. Since $S_\eta^I(0)=Z_i(1-A_i)$ for $\eta=0$, it indicates that A_i is the fractional oscillator strength contributed by discrete excitations. The sum rule for the $\mu=-1$ moment is satisfactorily fitted to

$$\begin{aligned}S_\eta^I(-1)=&\{[1-(1+\eta^2/4)^{-4}]/\eta^2\}\\&\times[S_\eta^I(0)-C_i\exp(-D_i\eta^2)\\&+F_i\exp(-G_i\eta^2)]\ ,\end{aligned} \tag{11}$$

with $C_i=0.05+0.01Z$, $0.2+0.06Z$, 0; $D_i=0.812$, 3.01, 0; $F_i=0$, $-0.06+0.09Z$, $0.0862ZE_{0i}/\mathcal{R}$; and $G_i=0$, 0.502, 2.013 for the $i=1s$, $2s$, and $2p$ subshells, respectively. In addition, the best fit to the sum rule for the $\mu=1$ moment is

$$\begin{aligned}S_\eta^I(1)=&S_\eta^I(0)[\eta^2+P_i\eta+Q_i\exp(-R_i\eta^2)\\&+S_i\exp(-0.456\eta^2)+T_i]\ ,\end{aligned} \tag{12}$$

with $P_i=0$, -0.7, 0.15; $Q_i=0.07+0.015Z$, $0.977-0.548Z$, $0.85-0.06Z$; $R_i=0.498$, 0.167, $-7.735+1.6Z$; $S_i=0$, 0, $-1.1+0.074Z$; and $T_i=1.333$, $2.432-0.12Z$, $1.9-0.1Z$ for the $i=1s$, $2s$, and $2p$ subshells, respectively.

Substituting Eqs. (1) and (4) into Eq. (5) by setting $\mu=-1$, 0, and 1, we obtain three equations containing three parameters A, B, and C. Combining these equations with Eqs. (10)–(12), we can solve these parameters with the aid of the following relations [10]:

$$S_{\rm CBC}(-1)=(ab+3ac+d)/(\pi\eta^2)\ , \tag{13}$$

$$S_{\rm CBC}(0)=[(a+4)b+3ac+d]/\pi\ , \tag{14}$$

$$\begin{aligned}S_{\rm CBC}(1)=&\{[a(\eta^2-4)+8\eta^2]b+3a(\eta^2+\tfrac{4}{3})c\\&+(\eta^2+\tfrac{4}{3})d\}/\pi\ ,\end{aligned} \tag{15}$$

$$\begin{aligned}S_{\rm CBC}(2)=&\{[a(\eta^2-12)+4(3\eta^2-4)]b\\&+[3a(\eta^2+4)+64]c\\&+(\eta^2+4)d\}\eta^2/\pi\ ,\end{aligned} \tag{16}$$

and

$$\begin{aligned}S_{\rm CBC}(3)=&\{[a(\eta^4-24\eta^2+16)+16\eta^2(\eta^2-4)]b\\&+[a(3\eta^4+24\eta^2-80)+256\eta^2]c\\&+(\eta^2+4)^2d\}\eta^2/\pi\ ,\end{aligned} \tag{17}$$

where

$$a=\eta^2-\epsilon_i ,$$

$$b=16\eta^3/3(a^2+4\eta^2)^2 ,$$

$$c=2\eta/3(a^2+4\eta^2) ,$$

and

$$d=\pi/2-\tan^{-1}(-a/2\eta) .$$

The ionization GOS of the sum-rule-constrained CBC model of Eq. (4) is thus determined.

III. RESULTS AND DISCUSSION

Figure 4 shows a plot of the ionization GOS for the boron 1s shell as a function of momentum transfer for two values of the energy transfer. The solid curves are results of the present work using the sum-role-constrained CBC model of Eq. (4) with sum rules given in Eqs. (10)–(12). For comparison, we plot also corresponding results obtained using the CBC model of Eq. (1) (dashed curves), the sum-rule-constrained CBC model with sum rules of Eqs. (6)–(8) (dot-dash curves), and the HFS matrix element method [11] (solid circles). It is seen that the CBC model works poorly at small momentum transfers. The sum-rule-constrained CBC model works successfully in predicting the ionization GOS at all momentum transfers. Since the 1s shell is fairly isolated and the hydrogenic model works quite well for that shell [20], Eqs. (6)–(8) are good approximations. This leads to the minor difference between GOS's calculated presently and by Tung [10]. The present results agree almost perfectly with the HFS GOS data.

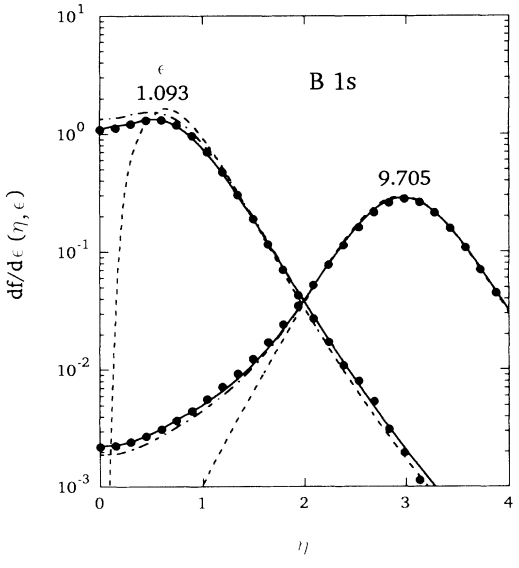

FIG. 4. The ionization GOS of the boron 1s shell as a function of momentum transfer for two values of the energy transfer. The solid curves, dot-dash curves, dashed curves, and solid circles represent, respectively, results of the sum-rule-constrained CBC model using Eqs. (4) and (10)–(12), the same model using Eqs. (4) and (6)–(8), the CBC model of Eq. (1), and the HFS matrix element method.

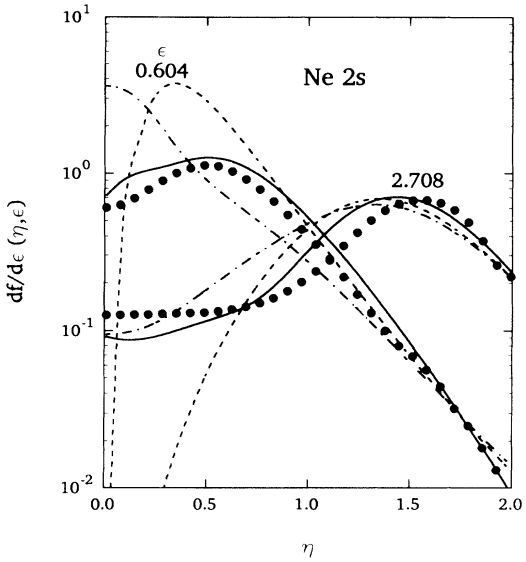

FIG. 5. The ionization GOS of the neon 2s-subshell as a function of momentum transfer for two values of the energy transfer. The solid curves, dot-dash curves, dashed curves, and solid circles represent, respectively, results of the sum-rule-constrained CBC model using Eqs. (4) and (10)–(12), the same model using Eqs. (4) and (6)–(8), the CBC model of Eq. (1), and the HFS matrix element method.

A similar plot for the neon 2s subshell is shown in Fig. 5. The superiority of the sum-rule-constrained CBC model over the CBC model in predicting the ionization GOS is quite clear. Results of the sum-rule-constrained CBC model corresponding to sum rules of Eqs. (10)–(12)

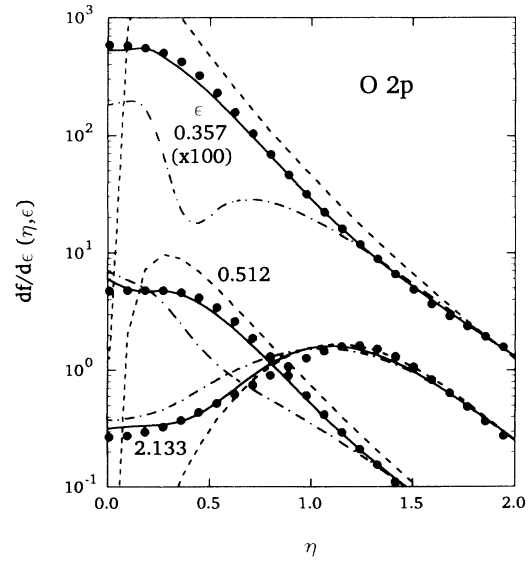

FIG. 6. The ionization GOS of the oxygen 2p subshell as a function of momentum transfer for several values of the energy transfer. The solid curves, dot-dash curves, dashed curves, and solid circles represent, respectively, results of the sum-rule-constrained CBC model using Eqs. (4) and (10)–(12), the same model using Eqs. (4) and (6)–(8), the CBC model of Eq. (1), and the HFS matrix element method.

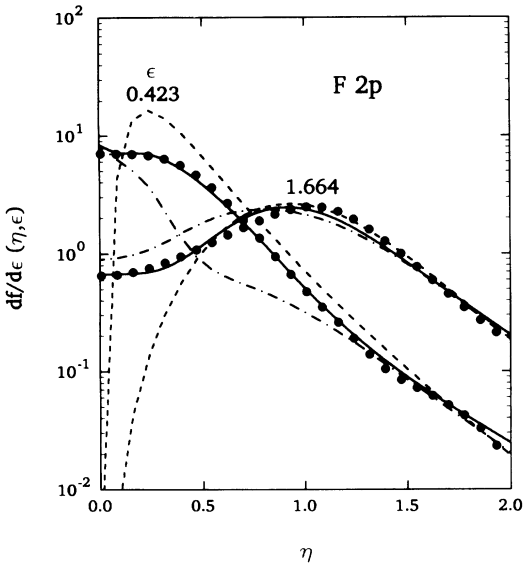

FIG. 7. The ionization GOS of the fluorine $2p$ subshell as a function of momentum transfer for several values of the energy transfer. The solid curves, dot-dash curves, dashed curves, and solid circles represent, respectively, results of the sum-rule-constrained CBC model using Eqs. (4) and (10)–(12), the same model using Eqs. (4) and (6)–(8), the CBC model of Eq. (1), and the HFS matrix element method.

are better than those of Eqs. (6)–(8) employed by Tung. The small deviation in ionization GOS's between the present work and the HFS matrix element method [11] is due to the limited number of sum rules applied and the error associated with analytical fittings adopted in Eqs. (10)–(12).

A comparison of ionization GOS's calculated using various methods for the $2p$ subshell of the oxygen atom is made in Fig. 6. Note that results for $\epsilon=0.0357$ are multiplied by 100 in order to distinguish them from other data in the figure. Here again the CBC model fails to predict ionization GOS's at small momentum transfers. The sum-rule-constrained CBC model is inadequate to predict ionization GOS's at small energy transfers if Eqs. (6)–(8) are employed. This model, however, is very well applied if sum rules of Eqs. (10)–(12) are used. A similar comparison for the $2p$ subshell of the fluorine atom is shown in Fig. 7. The same conclusions may be drawn regarding the applicability of the various methods. At any rate, the present results agree quite well with the HFS data.

IV. CONCLUSIONS

A sum-rule-constrained CBC model has been constructed to evaluate ionization GOS's of atomic subshells. This model was applied previously [10] using sum rules derived from several approximations. Although such an application remedied the failure of the CBC model in estimating ionization GOS at small momentum transfers, it worked only fairly for the $1s$ and $2s$ subshells and poorly for the $2p$ subshell. In the present work, we have reconstructed the sum-rule-constrained CBC model by employing improved sum rules obtained from the HFS matrix element method. The reconstructed model has been successfully applied to ionization GOS's of the K and L shells. The agreement on ionization GOS's between the present work and the HFS matrix element data was excellent for all momentum and energy transfers.

ACKNOWLEDGMENTS

This research was supported by the National Science Council of the Republic of China under Contract No. NSC80-0208-M009-10.

[1] R. F. Egerton, *Electron Energy-Loss Spectroscopy* (Plenum, New York, 1986).
[2] C. J. Powell, in *Electron Impact Ionization,* edited by T. D. Mark, and G. H. Dunn (Springer-Verlag, Wien, New York, 1985), p. 198.
[3] H. Bethe, Ann. Phys. (Leipzig) **5**, 325 (1930).
[4] M. R. H. Rudge, Rev. Mod. Phys. **40**, 564 (1968).
[5] L. Vriens, in *Case Studies in Atomic Collision Physics I,* edited by E. W. McDaniel and M. R. C. McDowell (North-Holland, Amsterdam, 1969), p. 335.
[6] S. M. Younger and T. D. Mark, in *Electron Impact Ionization,* edited by T. D. Mark and G. H. Dunn (Springer-Verlag, Wien, New York, 1985), p. 24.
[7] J. Lindhard and M. Scharff, K. Dan. Vidensk. Selsk. Mat. Fys. Medd. **27**, 1 (1953).
[8] C. J. Tung, J. C. Ashley, and R. H. Ritchie, Surf. Sci. **81**, 427 (1979).
[9] C. M. Kwei, T. L. Lin, and C. J. Tung, J. Phys. B **21**, 2901 (1988).
[10] C. J. Tung, Phys. Rev. A **22**, 2550 (1980).
[11] E. J. McGuire, Phys. Rev. A **3**, 267 (1971).
[12] S. T. Manson, Phys. Rev. A **6**, 1013 (1972).
[13] J. L. Dehmer, M. Inokuti, and R. P. Saxon, Phys. Rev. A **12**, 102 (1975).
[14] B. B. Robinson, Phys. Rev. **140**, A764 (1965).
[15] D. Liljequist, J. Phys. D **16**, 1567 (1983).
[16] M. Inokuti, Rev. Mod. Phys. **43**, 297 (1971).
[17] E. J. McGuire, J. M. Peek, and L. C. Pitchford, Phys. Rev. A **26**, 1318 (1982).
[18] E. J. McGuire, Phys. Rev. A **28**, 49 (1983).
[19] U. Fano and J. W. Cooper, Rev. Mod. Phys. **40**, 441 (1968).
[20] C. J. Tung and R. H. Ritchie, Phys. Rev. B **16**, 4302 (1977).